THE JOURNAL OF
PHYSICAL CHEMISTRY A

Article

pubs.acs.org/JPCA

Photoinduced Nonadiabatic Decay and Dissociation Dynamics of Dimethylnitramine

Xuhui Zhuang,[†,‡] Jun Wang,[†] and Zhenggang Lan*,[†,‡,§,∥]

[†]Qingdao Institute of Bioenergy and Bioprocess Technology, Chinese Academy of Sciences, 189 Songling Road, Qingdao, 266101 Shandong, P. R. China

[‡]University of Chinese Academy of Sciences, Beijing 100049, P. R. China

[§]Key Laboratory of Biobased Materials, Qingdao Institute of Bioenergy and Bioprocess Technology, Chinese Academy of Sciences, Qingdao, 266101 Shandong, P. R. China

[∥]Qingdao Key Laboratory of Solar Energy Utilization and Energy Storage Technology, Qingdao Institute of Bioenergy and Bioprocess Technology, Chinese Academy of Sciences, Qingdao, 266101, Shandong, P. R. China

Supporting Information

ABSTRACT: Dimethylnitramine (DMNA) is a prototype system used in the investigation of the unimolecular decomposition mechanism of the nitramine-compound family. The photoinduced excited-state nonadiabatic processes and successive unimolecular dissociation of DMNA were investigated by trajectory surface-hopping dynamics at the semiempirical OM2/MRCI level. Two S_1/S_0 conical intersections ($CI_{01\alpha}$ and $CI_{01\beta}$) were found to play essential roles in the nonadiabatic decay dynamics of DMNA. After the $S_1 \rightarrow S_0$ decay, the excess kinetic energy finally results in the cleavage of the N−N bond in the ground electronic state. The two reaction channels through $CI_{01\alpha}$ and $CI_{01\beta}$ show differences in molecular motions and decay features. The trajectories passing $CI_{01\alpha}$ can hop one or several times, and the intramolecular vibrational energy transfer in the ground state takes place before dissociation, whereas trajectories following the $CI_{01\beta}$ channel mainly dissociate directly after only one $S_1 \rightarrow S_0$ hop.

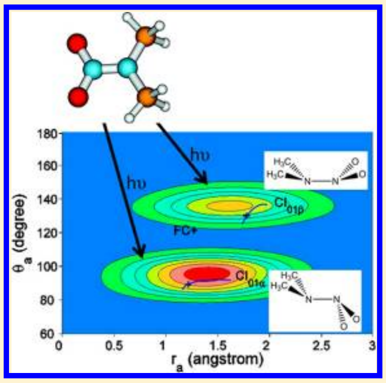

1. INTRODUCTION

As energetic materials, members of the nitramine-compound family, including 1,3,5-trinitro-1,3,5-triazacyclohexane (RDX), 1,3,5,7-tetranitro-1,3,5,7-tetraazacyclooctane (HMX), and dimethylnitramine (DMNA), are widely utilized as explosives and fuels, because they can store large amounts of releasable energy. Thus, over the past several decades, these nitramine compounds have been the focus of great research interest from both the experimental and theoretical points of view.[1−7] To fully understand how chemical energy in these materials converts into mechanical energy, many efforts have been made to study the mechanism of energy release through unimolecular decomposition.[8−15] Many earlier works focused on the thermal reactions of the nitramine family, particularly their dissociation in the ground electronic state.[16−22]

In recent years, the excited-state processes of the nitramine family have also attracted much research interest. In experimental studies, several different photolysis products (NO_2, CH_3ONO, CH_2O, CH_3NO, NO, and ON_2) have been observed.[23−25] The probability of obtaining different products can be modified by varying the experimental conditions. This indicates that the photochemistry of the nitramine family is very rich. Theoretically, the electronic excitations and excited-state reaction mechanisms of these compounds have been examined at different levels of electronic-structure theories. These studies suggest that nonadiabatic transitions between different electronic states play an essential role.[26−29]

As one of the simplest compounds in the nitramine family, DMNA has attracted broad research interest. Early work on DMNA confirmed its very short excited-state lifetime on the basis of its very broad absorption spectra. Furthermore, Mialocq and Stephenson[30] and McQuaid et al.[12] showed that the photoinduced dissociation products (ON_2, OH, NO, NO_2) are highly dependent on the laser-excitation wavelength. Many experimental investigations have focused on the dynamics starting from the second excited state S_2 because of its strong absorption. For example, Bernstein and co-workers performed a systematic exploration of the photoinduced dynamics of DMNA.[6,7,13] By the combination of experimental and theoretical studies, they found that (1) nonadiabatic transitions at the S_2/S_1 and S_1/S_0 conical intersections (CIs) play essential roles in the excited-state processes of DMNA, (2) significant nitro−nitrite isomerization is responsible for the decomposition of DMNA, and (3) the major product is NO. At room temperature and in low-collision environments, the isomerization mechanism is still valid, while the channel to generate

Received: March 3, 2013
Revised: May 10, 2013
Published: May 14, 2013

© 2013 American Chemical Society dx.doi.org/10.1021/jp402180p | J. Phys. Chem. A 2013, 117, 4785−4793

NO_2 and $N(CH_3)_2$ starts to be important because of the high diffusive ability of the products.

With the development of technology, the study of the photoinduced dynamics of DMNA starting from its lowest electronic excited state has become accessible. Using time-resolved pump−probe spectroscopy, Guo et al.[14] suggested that the S_1 state of DMNA undergoes an ultrafast single-exponential decay (lifetime = 50 ± 16 fs). Through the combination of experimental observations and theoretical calculations, they confirmed that the ultrafast decay of the S_1 state is due to the nonbarrier reaction pathway from the Franck−Condon (FC) region to the S_1/S_0 CI. They also proposed that, after $S_1 \rightarrow S_0$ decay, the bending motion of NO_2 is highly excited. Afterward, intramolecular vibrational energy transfer finally leads to the cleavage of the N−N bond. Their proposed mechanism of DMNA dissociation in the S_0 state is consistent with previous theoretical work by Sumpter and Thompson,[16] who predicted the key role of the NO_2 bending motion during N−N bond cleavage in thermal reactions.

Although many studies have been performed in an effort to unravel the interplay between the nonadiabatic dynamics and the dissociation of DMNA, it is still difficult to examine all of the details from experimental works and reaction-path calculations, particularly because of the complex nature of the dissociation products. Thus, it is necessary to directly simulate the excited-state dynamics of DMNA from the theoretical point of view, which would certainly bring a more precise understanding of the role of conical intersections in the photoinduced dissociation of DMNA. For this purpose, we performed nonadiabatic dynamics simulations of DMNA using the on-the-fly surface-hopping method.[31−33] The semiempirical OM2/MRCI method was employed to treat the relevant electronic states and their couplings, because many benchmark calculations showed that this method can provide a reasonable compromise between computational cost and accuracy.[34−36] Although it was reported that the OM2/MRCI method might not always give excellent descriptions of some systems,[37] nonadiabatic dynamics simulations at the OM2/MRCI level should still be a powerful and meaningful tool after careful benchmark calculations.[38−42] For benchmark reasons, high-level electronic calculations were also performed. As our first step to understand the nonadiabatic dynamics of the nitramine family, the current work focused on only the photoinduced reactions of DMNA from its first electronic excited state (S_1).

This article is organized as follows: In section 2, we address the computational details, including the OM2/MRCI method and the surface-hopping method. To test the accuracy of the OM2/MRCI method, ab initio and density functional theory (DFT)/time-dependent density functional theory (TDDFT) methods were also applied for benchmarking. In section 3, the results including the potential energy (PE) surface and nonadiabatic dynamics are discussed in detail. The last section summarizes the whole work.

2. COMPUTATIONAL DETAILS

In the current work, electronic-structure calculations and nonadiabatic dynamics simulation were mainly treated at the semiempirical level of theory. All semiempirical calculations were performed using the development version of the MNDO99 program.[43] For benchmark reasons, ab initio and DFT/TDDFT calculations were also performed at critical points. The TURBOMOLE program[44] was used in these benchmark calculations.

2.1. Semiempirical Method. The semiempirical electronic Hamiltonian was constructed within the framework of the orthogonalization model 2 (OM2) method.[34−36] Excited-state wave functions were described by the multireference configuration interaction (MRCI) method.[45] At the OM2/MRCI level, the potential energies of relevant electronic states, their gradients, and their nonadiabatic couplings were calculated analytically. The self-consistent field (SCF) calculations were performed according to the restricted open-shell Hartree-Fork (ROHF) formalism, which provides a reasonable description of excited-state wave functions.[46] In the MRCI expansion, three references (closed-shell and single and double HOMO−LUMO excitations) were used to build all configurations. All single and double excitations from these three references were included in the configuration-interaction treatment. The active space (AS) in the MRCI included 10 electrons in 9 orbitals [(10,9)]: one σ orbital, two π orbitals, two nonbonding orbitals, one π^* orbital, and three σ^* orbitals. This active space gives data that are consistent with results obtained using high-level theories, such as complete-active-space self-consistent field (CASSCF) with a similar AS size.[14] The slightly different AS used here with respect to the previous CASSCF work is mainly due to the smooth description of the excited-state PE surface.

Geometry optimizations of the ground-state and excited-state minima were performed using the Newton−Raphson iteration scheme. The minimum-energy structures of conical intersections were obtained using the Lagrange−Newton method.[47−49] Reaction pathways between the ground-state minimum and the relevant CIs were constructed by constrained optimization on the S_1 state. The CI seams were also located by the constrained CI optimization along the fixed N−N distance.

2.2. Nonadiabatic Dynamics. The photoinduced nonadiabatic decay dynamics was studied by trajectory-surface-hopping simulations at the OM2/MRCI level. The nonadiabatic transition was treated with Tully's fewest-switches algorithm. The initial sampling was composed of two successive steps, and all technical details can be found in refs 31−33 and 50. A set of 200 initial conditions (geometries and velocities) were randomly selected from a preliminary 10-ps Born−Oppenheimer molecular dynamics on the S_0 surface at 300 K. Then, initial conditions were created by putting these snapshots into the S_1 state vertically. All relevant energies, gradients, and nonadiabatic couplings were calculated analytically in an "on-the-fly" manner. The step time was 0.1 fs for nuclear motion and 0.001 fs for electronic propagation. To check the short-time nonadiabatic features and examine the long-time behavior of molecular motions, dynamics up to both 1 and 2 ps were calculated.

2.3. High-Level Calculations. To test the accuracy of the data calculated at the semiempirical level, ab initio and DFT calculations were also performed at the critical points. The B3LYP,[25,51,52] PBE,[53] and PBE0[54−57] functionals with the def2-SVP basis set[58,59] were used in DFT/TDDFT calculations. In ab initio calculations, the RI-MP2 method[60−63] with the SVP basis set[64,65] was used to optimize the S_0 minima. Then, the excited states were treated at the ADC(2)/SVP level of theory.[66]

3. RESULTS

The molecular structure of DMNA is shown in Figure 1. The geometry parameters used in the study of photoinduced processes are listed in Table 1. In this table, bond lengths N1−

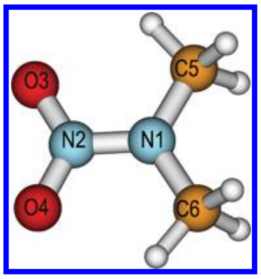

Figure 1. Molecular structure of DMNA.

Table 1. Important Internal Coordinates

label	internal coordinate
r_a	distance N1−N2
r_b	distance N2−O3
r_c	distance N1−C5
θ_a	angle O3−N2−O4
θ_b	angle C5−N1−C6
τ_a	dihedral angle N1−N2−O3−O4
τ_b	dihedral angle N2−N1−C5−C6

N2, N2−O3, and N1−C5 are described by r_a, r_b, and r_c, respectively. The bond angles O3−N2−O4 and C5−N1−C6 are represented as θ_a and θ_b, respectively. The dihedral angles N1−N2−O3−O4 (τ_a) and N2−N1−C5−C6 (τ_b) describe the pyramidalizations at the N2 and N1 atoms, respectively.

3.1. Potential Energy Surface. Two S_0 minimum-energy structures of DMNA were located at the OM2/MRCI level (Figure 2). The frequency analysis shows that both of them are real minima. The first S_0 minimum, $(S_0)_{\min\alpha}$, displays a perfectly planar structure with C_{2v} symmetry, as reported previously.[67,68] The second S_0 minimum, $(S_0)_{\min\beta}$, is located only slightly higher (0.01 eV) than $(S_0)_{\min\alpha}$; see Table 2. Weak pyramidalization at N1 atom ($\tau_b = -156.0°$) is observed at $(S_0)_{\min\beta}$, which displays C_s symmetry. We note that the PE surface between two S_0 minima is very flat. (See Figure S-1 of the Supporting Information.)

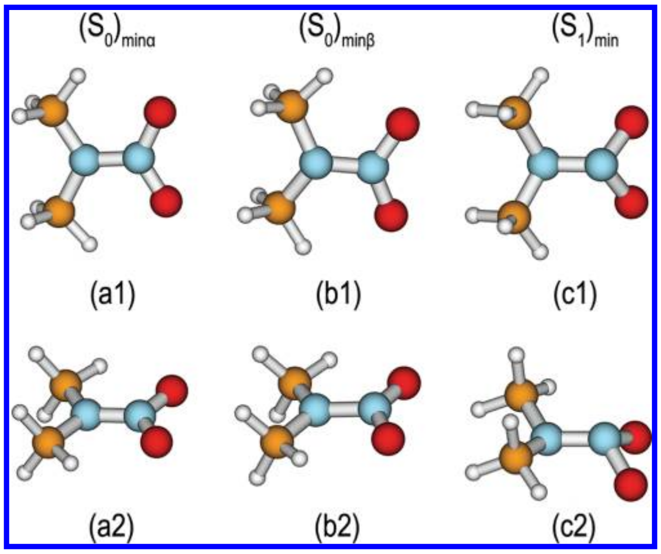

Figure 2. Optimized geometries of two ground-state minima $[(S_0)_{\min\alpha}, (S_0)_{\min\beta}]$ and one lowest singlet excited-state minimum $(S_1)_{\min}$ of DMNA obtained at the semiempirical OM2/MRCI level of theory with AS(10,9): (a1,b1,c1) top views and (a2,b2,c2) side views.

At the OM2/MRCI level, the vertical energies of the lowest singlet excited state S_1 at $(S_0)_{\min\alpha}$ and $(S_0)_{\min\beta}$ are 4.31 and 4.33 eV, respectively. S_1 corresponds to the HOMO → LUMO transition with $n\pi^*$ character, and they are all in good agreement with the available experimental absorption value of 4.57 eV (271 nm).[14]

Both the minima were optimized at the DFT and RI-MP2 levels. In these cases, $(S_0)_{\min\beta}$ is the global minimum, and the energy difference between the two S_0 minima is still rather small. At the TDDFT level, the $S_0 \rightarrow S_1$ transition energies at $(S_0)_{\min\alpha}$ and $(S_0)_{\min\beta}$ are in the ranges of 4.52−4.80 and 4.61−4.81 eV, respectively. Similar data were also obtained at the ADC(2) level. Interestingly, the pure functional PBE seems to give better performance than the hybrid functionals B3LYP and PBE0. Given the general deviations of TDDFT and ADC(2), our OM2/MRCI data are acceptable.

Starting from the ground-state minimum, only one S_1 minimum is located at the OM2/MRCI level. The $(S_1)_{\min}$ is characterized by the pyramidalization motions at N2 and N1 atoms along opposite directions ($\tau_a = -125.1°$, $\tau_b = -146.9°$). At $(S_1)_{\min}$, the energy gap between the S_1 and S_0 states is 0.51 eV. The $(S_1)_{\min}$ state with a similar geometry can also be found at the TDDFT level. We observed that the TDDFT method tends to predict less distortion of the $(S_1)_{\min}$ geometry and a higher S_1 energy than the OM2/MRCI method. However, the topologies of the $(S_1)_{\min}$ geometries at the two levels are similar (see Figure S-2, Supporting Information). This means that the OM2/MRCI method should, in principle, give a qualitatively correct description of the $(S_1)_{\min}$ state.

Two S_1/S_0 conical-intersection minima were located at the OM2/MRCI level that differed by two key internal coordinates: the N−N bond distance and the pyramidalization at the two N atoms. (See Figure S-3, Supporting Information.)

The first S_1/S_0 conical-intersection minimum, $\mathrm{CI}_{01\alpha}^{\mathrm{m}}$, lies 3.09 eV above the global ground-state minimum $[(S_0)_{\min\alpha}]$. Pronounced N−N stretching is not observed at $\mathrm{CI}_{01\alpha}^{\mathrm{m}}$ (r_a = 1.38 Å) with respect to $(S_0)_{\min\alpha}$. The most striking feature of $\mathrm{CI}_{01\alpha}^{\mathrm{m}}$ is the presence of rather strong pyramidalizations at the N2 ($\tau_a = 121.5°$) and N1 ($\tau_b = 144.3°$) atoms, whereas the two pyramidalization modes are aligned in opposite directions with respect to the molecular plane. $\mathrm{CI}_{01\alpha}^{\mathrm{m}}$ also exhibits a pronounced O−N−O bending motion with respect to $(S_0)_{\min\alpha}$ ($\theta_a = 88.4°$; see Figure 3).

The second S_1/S_0 conical-intersection minimum, $\mathrm{CI}_{01\beta}^{\mathrm{m}}$, is located at 2.12 eV relative to $(S_0)_{\min\alpha}$. The most significant feature of this conical intersection is that the N−N bond becomes very long (r_a = 1.75 Å). This means that a strong N−N stretching motion is necessary to access $\mathrm{CI}_{01\beta}^{\mathrm{m}}$ from the Franck−Condon (FC) region. Pronounced pyramidalizations at the N2 ($\tau_a = 134.1°$) and N1 ($\tau_b = -153.6°$) atoms are also observed at $\mathrm{CI}_{01\beta}^{\mathrm{m}}$, although they point in the same direction with respect to the molecular plane. Both the pyramidalizations and the bending motion of the O−N−O group at $\mathrm{CI}_{01\beta}^{\mathrm{m}}$ are less pronounced than those at $\mathrm{CI}_{01\alpha}^{\mathrm{m}}$.

To obtain the further information on the S_1/S_0 crossing, CI seams were constructed by CI constrained optimization following the N−N distance (r_a) (for typical geometries with longer N−N bond distances, see Figure S-4 of the Supporting Information). For the range of r_a values (1.33−1.73 Å), $\mathrm{CI}_{01\alpha}$ preserves its nonplanar character, whereas such optimization faces nonconvergence problem when r_a is longer than 1.73 Å. For the same reason, the $\mathrm{CI}_{01\beta}$ seam can be constructed up to 1.92 Å. With increasing r_a, the nonplanar character becomes

Table 2. Adiabatic Energies (eV) and Vertical Energies (in Brackets) of Electronic States at $(S_0)_{\min\alpha}$, $(S_0)_{\min\beta}$, and $(S_1)_{\min}$

geometry	state	B3LYP	PBE	PBE0	RI-MP2-ADC(2)	OM2/MRCI
$(S_0)_{\min\alpha}$	S_0	0.05 [0.00]	0.02 [0.00]	0.04 [0.00]	0.10 [0.00]	0.00 [0.00]
	S_1	4.75 [4.70]	4.54 [4.52]	4.84 [4.80]	4.71 [4.61]	4.31 [4.31]
$(S_0)_{\min\beta}$	S_0	0.00 [0.00]	0.00 [0.00]	0.00 [0.00]	0.00 [0.00]	0.01 [0.00]
	S_1	4.72 [4.72]	4.61 [4.61]	4.81 [4.81]	4.59 [4.59]	4.34 [4.33]
$(S_1)_{\min}$	S_0	1.90 [1.90]	1.91 [1.91]	1.97 [1.97]	–	2.54 [2.45]
	S_1	3.62 [3.62]	3.38 [3.38]	3.81 [3.81]	–	3.05 [3.05]

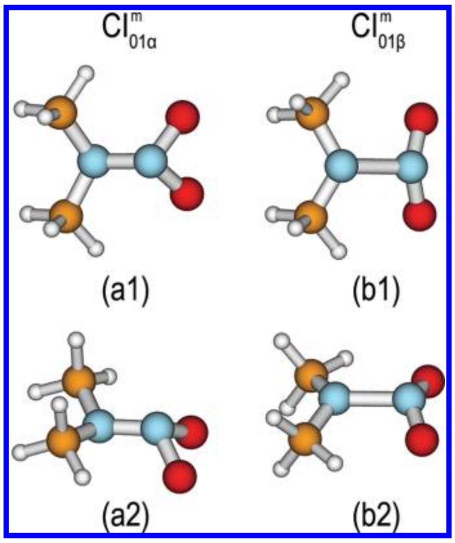

Figure 3. Geometries of two optimized S_1/S_0 conical-intersection minima of DMNA at the OM2/MRCI level with AS(10,9). The energies of $CI^m_{01\alpha}$ and $CI^m_{01\beta}$ are 3.09 and 2.12 eV, respectively. (a1,b1) Top views and (a2,b2) Side views.

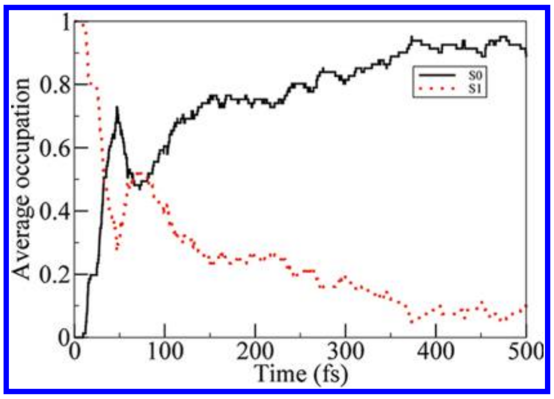

Figure 4. Time-dependent average fractional occupation of electronic states.

weaker, and finally, a planar geometry is reached (τ_a = 180.0°, τ_b = 180.0°) for $CI_{01\beta}$. Relative structure parameters of these geometries are reported in Table S-1 (Supporting Information).

Potential energy surfaces between the FC geometry $[(S_0)_{\min\alpha}]$ and the two S_1/S_0 CIs were constructed using constrained optimization on the S_1 state by fixing key reaction coordinates. For both pathways, no barrier was observed; see Figure S-5 of the Supporting Information for details. This suggests that both $CI^m_{01\alpha}$ and $CI^m_{01\beta}$ should be responsible for the nonadiabatic channels in the photoinduced reaction of DMNA.

3.2. Nonadiabatic Dynamics of DMNA. Ground-state molecular dynamics simulations were run to generate a set of snapshots for initial sampling. To test whether a 10-ps molecular dynamics run in the ground state is long enough for initial sampling, the statistical data for geometry distribution were examined along the molecular-dynamics trajectory at different time durations (see Figure S-6, Supporting Information). After 6 ps, the distribution functions of important geometric coordinates (r_a, τ_a, and τ_b) became rather stable. Also, concerning the size of the current system, it is reasonable to believe that 10 ps of molecular dynamics in the electronic ground state is long enough to span all important regions of the full phase space. Because the two S_0 minima have very similar energies and no barrier between them (see Figure S-1 of the Supporting Information for details), such an approach should, in principle, cover a reasonable geometric region for sampling.

After excitation to S_1, DMNA displays ultrafast $S_1 \rightarrow S_0$ decay; see Figure 4. Within the first 35 fs, 50% of the trajectories jumped to the S_0 state. Interestingly, the recurrence of the S_1 population was observed, and about 25% of the trajectories jumped back to the S_1 state at 47 fs. Afterward, the S_1 population decayed almost monotonically, and no obvious recurrence occurred. After 400 fs, more than 90% of the trajectories hopped to S_0, and the decay was essentially over. The plot of the average fractional occupation exhibits two interesting phenomena. The first is the ultrafast decay of S_1 population. More than 60% of the trajectories decayed to S_0 within 100 fs. This ultrafast decay is in good agreement with the experimental results (lifetime of 50 ± 16 fs).[14] It is well-known that the natural broadening of absorption spectra can be explained by the uncertainty principle correlating the excited-state lifetime and its energy. Thus, the rather short lifetime gives a large energy uncertainty and a broad band.[69] This explains the rather broad absorption of the S_1 state in DMNA.[70] The second is the recurrence of the S_1 population in the early stage of the dynamics. This phenomenon was not observed in the experimental study, which might be because the recurrence time is too short to be detected.

To understand the roles of conical intersections in the reaction dynamics, the nonadiabatic decay of DMNA was further examined by checking two key geometric parameters (r_a and θ_a) at the first S_1/S_0 hopping event, as shown in Figure 5.

Starting from the FC region, the system moves on the S_1 state and accesses two CIs ($CI_{01\alpha}$ and $CI_{01\beta}$) quickly, where the first $S_1 \rightarrow S_0$ hop takes place. The probabilities of passing $CI_{01\alpha}$ and $CI_{01\beta}$ are similar for the first $S_1 \rightarrow S_0$ hop; see Figure 5. This indicates that the two conical intersections play equivalent roles in the nonadiabatic dynamics of DMNA. The $CI_{01\alpha}$ seam is almost parallel to the N−N bond stretching motion. Thus, we expect that the approach to the $CI_{01\alpha}$ seam from the FC region does not necessarily require N−N stretching, whereas pyramidalization must be involved. In contrast to the $CI_{01\alpha}$ seam, the $CI_{01\beta}$ seam is partially perpendicular to the N−N stretching motion. Thus, the N−N bond must be extended before the $CI_{01\beta}$ seam is reached. We could not obtain the profile of the whole CI seam, because the constrained optimizations of conical intersections did not converge at

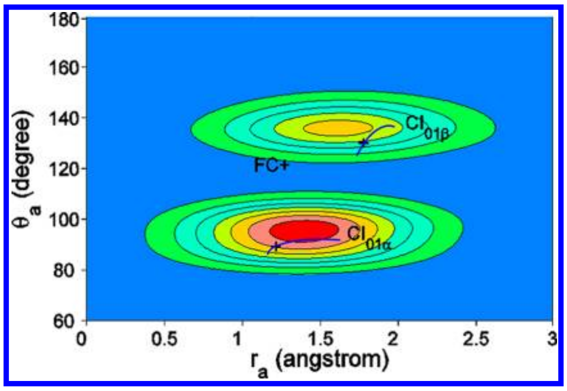

Figure 5. Geometric distribution at the first hops (over all trajectories) as functions of r_a and θ_a. Solid lines represent the two conical-intersection seams $CI_{01\alpha}$ and $CI_{01\beta}$. The minima ($CI^m_{01\alpha}$ and $CI^m_{01\beta}$) of these two CI seams are marked by crosses (+). The label FC refers to the Franck−Condon point.

long N−N distances. However, the current data are sufficient to examine the basic features of the CI seams and explain the nonadiabatic reaction channels.

After the investigation of the first $S_1 \rightarrow S_0$ hops, the next task was to clarify the final reaction products and their dependence on different conical-intersection pathways. The branching ratios of all reaction channels are shown in Figure 6.

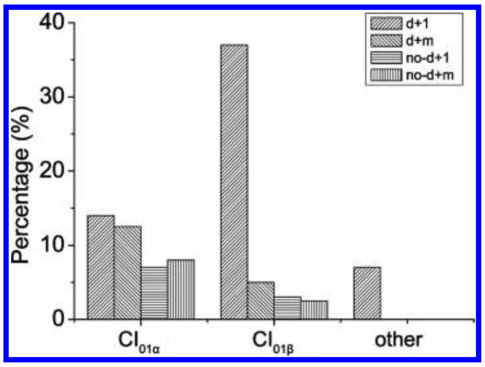

Figure 6. Percentage distribution of trajectories toward different reaction channels: d, trajectories display dissociation up to 1 ps; d + 1, trajectories that dissociate directly after only one $S_1 \rightarrow S_0$ hop; d + m, trajectories that hop down and up several times before dissociation; no-d + 1, trajectories that have one $S_1 \rightarrow S_0$ hop and do not dissociate at the end of simulation; no-d + m, trajectories that hop several times and do not dissociate.

For a majority of the trajectories, dissociation took place after the system finally jumped back to the S_0 state. For both the $CI_{01\alpha}$ and $CI_{01\beta}$ channels, N−N bond cleavage was observed, and the final products were NO_2 and $N(CH_3)_2$. However, the two CI channels showed rather different dynamic features. Here, we provide only the important data in Figure 6 for analysis; more details on the branching ratios can be found in Table S-2 (Supporting Information).

About 42% of all of the trajectories passed $CI_{01\alpha}$ during their first hops. Afterward, these trajectories had different destinations, and most of them went to dissociation. Overall, 14% of the trajectories dissociated directly after only one $S_1 \rightarrow S_0$ hop, whereas 13% of the trajectories hopped more than once before dissociation. Only a minor fraction of the trajectories did not ultimately dissociate. Also in Figure 6, it is noted that 48% of all trajectories accessed $CI_{01\beta}$ during their first hops. Significantly differing from the $CI_{01\alpha}$ channel, most trajectories (37%) here dissociated directly without any rehopping. Only a few of trajectories exhibited several hops. We also observed other reaction channels, although their contributions were so minimal that we did not consider them. For both the $CI_{01\alpha}$ and $CI_{01\beta}$ channels, dissociation occurred after the last hop, meaning that these trajectories should dissociate on the S_0 state rather than the S_1 state.

To test the convergence of the branching ratio toward different products in the dynamics simulations, we also performed an independent set of nonadiabatic dynamics simulations up to 2 ps, and the results were essentially same. (See Figure S-7 of the Supporting Information for details.)

To understand why the final reaction channels were strongly dependent on the conical intersections, typical trajectories of the two reaction channels were examined in detail.

For trajectories passing $CI_{01\alpha}$, it is important to understand why many of them dissociated after several hops. Thus, one such typical trajectory is plotted in Figure 7a−f. Within the first 100 fs, the molecule hopped several times between S_0 and S_1 through $CI_{01\alpha}$ (Figure 7b,f) and then finally decayed to S_0. The reasons for the multiple hops can be understood by examining the involved internal coordinates (Figure 7c−f). In the early stages of the dynamics, only the strong pyramidalization at the N2 atom (τ_a in Figure 7c) was observed, whereas the N−N distance did not increase obviously. Thus, the trajectory accessed $CI_{01\alpha}$ repeatedly, resulting in several hops. The feature of this typical trajectory is consistent with the geometric distribution of the first hopping events (see Figure 5). From the discussion regarding Figure 5, it is expected that the strong pyramidalization at the N2 atom, instead of the N−N stretching motion, drives trajectories moving toward $CI_{01\alpha}$. As far as the trajectory decaying to the S_0 state, the energy flowed from pyramidalization at the N2 atom to pyramidalization at the N1 atom (Figure 7c,d). After 700 fs, the elongation of the N−N distance started to appear, leading to dissociation. This implies that intramolecular vibrational energy transfer on the ground state is necessary for dissociation.

At this point, the dynamics for this type of trajectory becomes rather clear. The profile of the S_1 surface generates a pyramidalization motion at the N2 atom instead of an initial N−N elongation, which might result in multiple hops at $CI_{01\alpha}$. Between the first and last hops, all jumps take place at $CI_{01\alpha}$, and $CI_{01\beta}$ is not involved at all. After the last $S_1 \rightarrow S_0$ hop, the vibrational energy flows from the pyramidalization motion at the N2 atom to the N−N stretching motion. This finally leads to dissociation and gives NO_2. This analysis can explain why this group of trajectories can experience one or several hops before the final dissociation. The number of hops at $CI_{01\alpha}$ should depend on the time scale of vibrational energy transfer.

To understand the mechanism of vibrational energy flows from the pyramidalization at the N2 atom to the N−N stretching motion, two-dimensional potential energy surfaces of the S_0 and S_1 states were constructed as functions of the N−N stretching coordinate and the pyramidalization angle (see Figure S-8, Supporting Information). On the S_0 state, these two vibrational motions can be described independently near the ground-state minimum region, whereas strong couplings between them exist in the case of large-amplitude molecular vibrations. After the trajectories (through $CI_{01\alpha}$) finally jump back to the S_0 state, the excess kinetic energy certainly results in a rather strong pyramidalization motion, and thus, the strong coupling region is accessible. As a result, vibrational energy flow

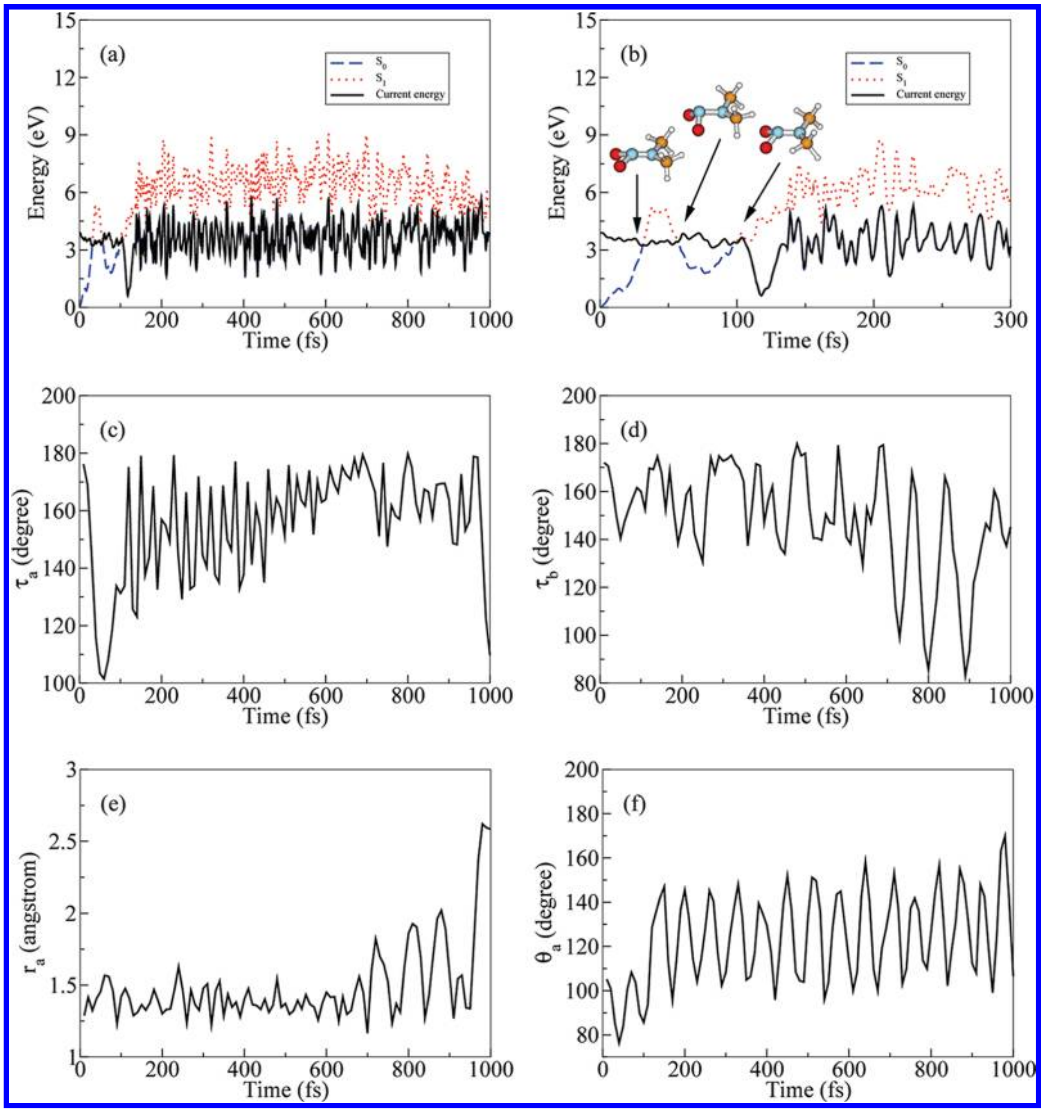

Figure 7. Time-dependent properties of a typical trajectory that passes the $CI_{01\alpha}$ seam and displays many hops: (a) potential energies of relevant electronic states over the entire simulation time (1000 fs); (b) potential energies within 300 fs for all hopping geometries; (c−f) geometric parameters (c) τ_a, (d) τ_b, (e) r_a, and (f) θ_a as functions of simulation time.

from the pyramidalization at the N2 atom to the N−N stretching motion becomes possible on the S_0 state. Similar vibrational energy transfer was noticed by Sumpter and Thompson, who investigated the thermal decomposition of DMNA.[16] Although previous studies have assumed the decisive role of the O−N−O bending motion in vibrational energy transfer, we prefer to propose that this NO_2 bending motion is mainly a result of pyramidalization at the N2 atom. If the vibrational energy transfer becomes very inefficient, dissociation might not take place. This can explain the small number of trajectories that did not dissociate within the simulated time scale (up to 2 ps). However, these nondissociated trajectories play only a minor role in the nonadiabatic dynamics of DMNA.

Most trajectories passing $CI_{01\beta}$ dissociated after only one $S_1 \rightarrow S_0$ hop. The underlying mechanism can be understood by checking a typical trajectory in Figure 8a−f. In this case, the N−N stretching motion is excited in the very earlier stage of the dynamics (Figure 8e). The elongation of the N−N bond brings the system into $CI_{01\beta}$, where the $S_1 \rightarrow S_0$ hop occurs. This observation is consistent with the discussion regarding Figures 3 and 5, because the N−N stretching motion becomes necessary when $CI_{01\beta}$ is accessible. After the $S_1 \rightarrow S_0$ hop, the excess vibrational energy in the N−N stretching motion leads directly to N−N bond cleavage, and product NO_2 is released. Thus, in this situation, direct dissociation takes place after only one $S_1 \rightarrow S_0$ hop at $CI_{01\beta}$. For the trajectories passing both $CI_{01\alpha}$ and $CI_{01\beta}$, dissociation occurs in the ground electronic state. Thus, dissociation takes place only after $S_1 \rightarrow S_0$ nonadiabatic decay. For most trajectories, we did not observe isomerization along the N−N bond or the formation of HONO. These two motions are supposed to be very important to the nonadiabatic dynamics of DMNA if the S_2 state represents the initial condition.[13,15,71]

4. CONCLUSIONS

In the current work, we studied the mechanism of the photoinduced chemical reactions of DMNA by nonadiabatic dynamics simulation at the OM2/MRCI(10,9) level. As a preliminary work, we focused on the nonadiabatic dynamics starting from the S_1 state and the successive dissociation after $S_1 \rightarrow S_0$ decays.

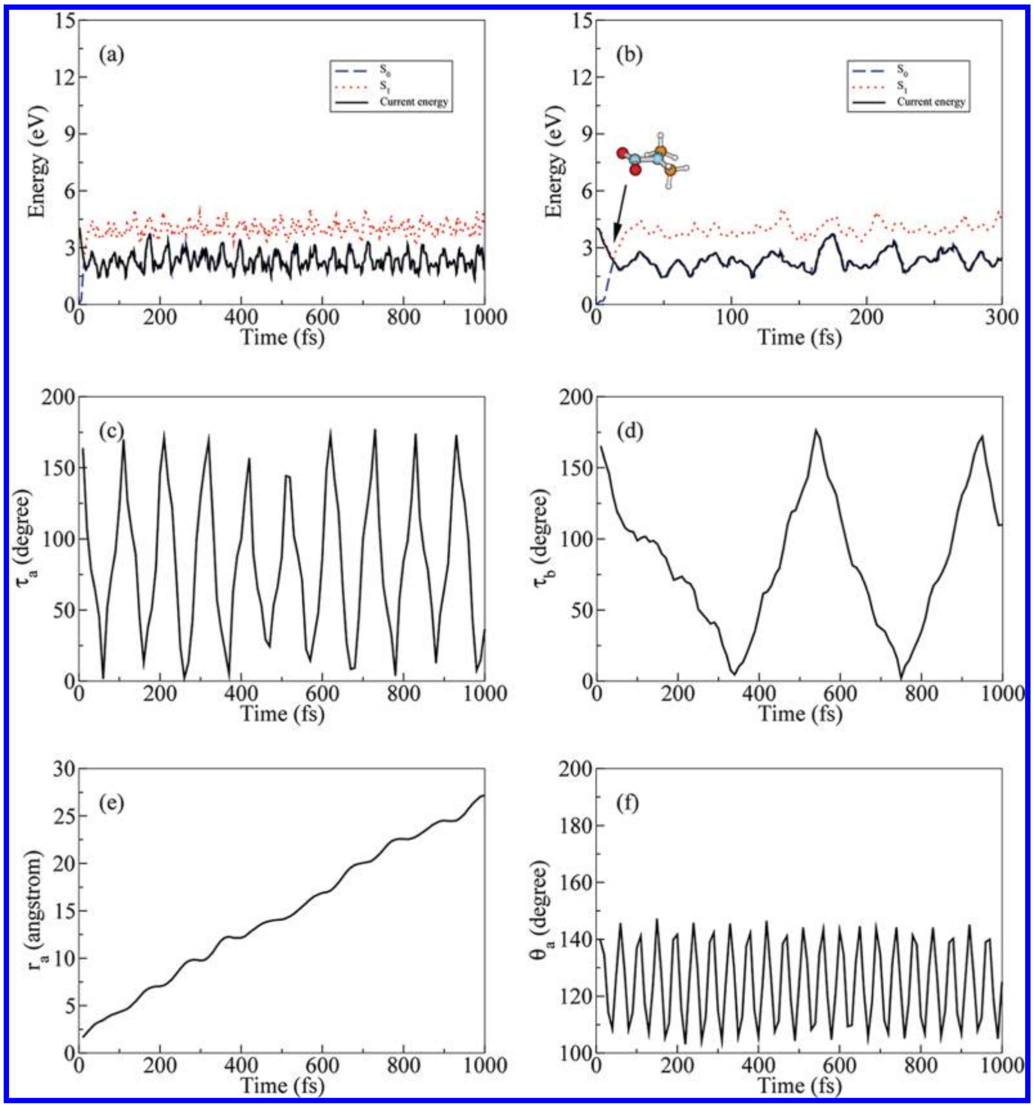

Figure 8. Time-dependent properties of a typical trajectory that passes the $CI_{01\beta}$ seam and displays one hop: (a) potential energies of relevant electronic states over the entire simulation time (1000 fs); (b) potential energies within 300 fs and the hopping geometry; (c−f) geometric parameters (c) τ_a, (d) τ_b, (e) r_a, and (f) θ_a as functions of simulation time.

Two S_1/S_0 CI minima were located at the OM2/MRCI-(10,9) level. The first one, $CI^m_{01\alpha}$, displays strong pyramidalizations at both the N2 and N1 atoms but in opposite directions, as well as a short N−N distance. The second CI minimum, $CI^m_{01\beta}$, is also characterized by pyramidalizations at N2 and N1 atoms but in the same direction. At $CI^m_{01\beta}$, N−N bond elongation is also observed.

In the surface-hopping simulation, the ultrafast decay process was observed within 100 fs. This explains the extremely short lifetime of the S_1 state in the experimental observations of Guo et al.[14] and the rather broad absorption line shape of the $S_0 \rightarrow S_1$ transition.[70] When the nonadiabatic decay finishes, the excess energy finally leads to unimolecular dissociation in the ground state. For most trajectories, the final products are NO_2 and $N(CH_3)_2$.

The two CIs play essentially equivalent roles in the nonadiabatic dynamics of DMNA, although the trajectories following these two channels show rather different features. Many trajectories passing $CI_{01\alpha}$ can hop one time or several times before the final dissociation. During this process, intramolecular vibrational energy transfer from pyramidalization at the N2 atom to N−N bond stretching is observed. For trajectories accessing $CI_{01\beta}$, N−N bond elongation should be necessary. As a result, direct dissociation is preferred after only one $S_1 \rightarrow S_0$ hop.

The current trajectory-surface-hopping simulations at the semiempirical OM2/MRCI level provide a reasonable description of the photoinduced reaction of DMNA with rather low computational cost. The results are consistent with those of available experimental and theoretical studies. In addition, we found many novel and interesting insights in the photoinduced dynamics of DMNA. We hope that these new findings will inspire further research interest in the excited-state dynamics of energetic materials.

■ ASSOCIATED CONTENT

Ⓢ Supporting Information

Typical structures at critical geometries (S_1 minimum and S_0/S_1 CIs), PE surfaces beween the FC point and two S_0/S_1 CIs and between two S_0 minima, branching ratios of reaction products in the nonadiabatic dynamics simulation, distributions at different time durations, two-dimensional PE surfaces, internal coordinates at critical geometries and geometry distribution of nonadiabatic dynamics, and Cartesian coordinates of all important geometries. This material is available free of charge via the Internet at http://pubs.acs.org.

■ AUTHOR INFORMATION

Corresponding Author

*Fax: +86-532-80662778. Tel.: +86-532-80662630. E-mail: lanzg@qibebt.ac.cn.

Notes

The authors declare no competing financial interest.

■ ACKNOWLEDGMENTS

This work was supported by the CAS 100 Talent Project, NSFC Project (Grants 21103213 and 91233106), and Director Innovation Foundation of CAS-QIBEBT. The authors thank Supercomputing Center, Computer Network Information Center, CAS, and the super computational center of CAS-QIBEBT for providing computational resources.

■ REFERENCES

(1) Oyumi, Y.; Rheingold, A. L.; Brill, T. B. Thermal Decomposition of Energetic Materials. 19. Unusual Condensed-Phase and Thermolysis Properties of a Mixed Azidomethyl Nitramine: 1,7-Diazido-2,4,6-trinitro-2,4,6-triazaheptane. *J. Phys. Chem.* **1987**, *91*, 920−925.

(2) Owens, F. J.; Sharma, J. X-ray Photoelectron Spectroscopy and Paramagnetic Resonance Evidence for Shock-Induced Intramolecular Bond Breaking in Some Energetic Solids. *J. Appl. Phys.* **1980**, *51*, 1494−1497.

(3) Zhao, X.; Hintsa, E. J.; Lee, Y. T. Infrared Multiphoton Dissociation of RDX in a Molecular Beam. *J. Chem. Phys.* **1988**, *88*, 801−810.

(4) Dick, J. J.; Mulford, R. N.; Spencer, W. J.; Pettit, D. R.; Garcia, E.; Shaw, D. C. Shock Response of Pentaerythritol Tetranitrate Single Crystals. *J. Appl. Phys.* **1991**, *70*, 3572−3587.

(5) Oxley, J. C.; Kooh, A. B.; Szekeres, R.; Zheng, W. Mechanisms of Nitramine Thermolysis. *J. Phys. Chem.* **1994**, *98*, 7004−7008.

(6) Guo, Y. Q.; Greenfield, M.; Bernstein, E. R. Decomposition of Nitramine Energetic Materials in Excited Electronic States: RDX and HMX. *J. Chem. Phys.* **2005**, *122*, 244310.

(7) Guo, Y. Q.; Greenfield, M.; Bhattacharya, A.; Bernstein, E. R. On the Excited Electronic State Dissociation of Nitramine Energetic Materials and Model Systems. *J. Chem. Phys.* **2007**, *127*, 154301.

(8) Flournoy, J. M. Thermal Decomposition of Gaseous Dimethylnitramine. *J. Chem. Phys.* **1962**, *36*, 1106.

(9) Lloyd, S. A.; Umstead, M. E.; Lin, M. C. Kinetics and Mechanism of the Thermal Decomposition of Dimethylnitramine at Low Temperatures. *J. Energ. Mater.* **1985**, *3*, 187−210.

(10) Oxley, J. C.; Hiskey, M.; Naud, D.; Szekeres, R. Thermal Decomposition of Nitramines: Dimethylnitramine, Diisopropylnitramine, and *N*-Nitropiperidine. *J. Phys. Chem.* **1992**, *96*, 2505−2509.

(11) Ling, Y.; Tang, Z.-H.; Xiao, H.-M. Molecular Orbital Studies of the Thermal Decomposition Mechanism of Dimethylnitramine. *Propellants, Explos., Pyrotech.* **1992**, *17*, 116−119.

(12) McQuaid, M. J.; Miziolek, A. W.; Sausa, R. C.; Merrow, C. N. Photodissociation of Dimethylnitramine at 248 nm. *J. Phys. Chem.* **1991**, *95*, 2713−2718.

(13) Bhattacharya, A.; Guo, Y. Q.; Bernstein, E. R. Experimental and Theoretical Exploration of the Initial Steps in the Decomposition of a Model Nitramine Energetic Material: Dimethylnitramine. *J. Phys. Chem. A* **2009**, *113*, 811−823.

(14) Guo, Y.; Bhattacharya, A.; Bernstein, E. R. Ultrafast S_1 to S_0 Internal Conversion Dynamics for Dimethylnitramine through a Conical Intersection. *J. Phys. Chem. A* **2011**, *115*, 9349−9353.

(15) Bhattacharya, A.; Bernstein, E. R. Nonadiabatic Decomposition of Gas-Phase RDX through Conical Intersections: An ONIOM-CASSCF Study. *J. Phys. Chem. A* **2011**, *115*, 4135−4147.

(16) Sumpter, B. G.; Thompson, D. L. Unimolecular Reaction Dynamics of Dimethylnitramine. *J. Chem. Phys.* **1988**, *88*, 6889−6897.

(17) Sumpter, B. G.; Thompson, D. L. Intramolecular Vibrational Relaxation from CH Stretching Modes in Dimethylnitramine. *J. Chem. Phys.* **1987**, *86*, 3301−3310.

(18) Smith, G. D.; Bharadwaj, R. K.; Bedrov, D.; Ayyagari, C. Quantum-Chemistry-Based Force Field for Simulations of Dimethylnitramine. *J. Phys. Chem. B* **1999**, *103*, 705−713.

(19) Smith, G. D.; Bharadwaj, R. K. Quantum Chemistry Based Force Field for Simulations of HMX. *J. Phys. Chem. B* **1999**, *103*, 3570−3575.

(20) Johnson, M. A.; Truong, T. N. High-Level ab Initio and Density Functional Theory Evaluation of Combustion Reaction Energetics: NO_2 and HONO Elimination from Dimethylnitramine. *J. Phys. Chem. A* **1999**, *103*, 8840−8846.

(21) Johnson, M. A.; Truong, T. N. Importance of Polarization in Simulations of Condensed Phase Energetic Materials. *J. Phys. Chem. B* **1999**, *103*, 9392−9393.

(22) Schweigert, I. V. Mechanisms of Condensed-phase Dissociation of Nitramines: A Density-Functional Study. *AIP Conf. Proc.* **2012**, *1426*, 1275−1278.

(23) Spears, K. G.; Brugge, S. P. Vibrationally Excited NO_2 from CH_3NO_2 and 2-$C_3H_7NO_2$ Photodissociation. *Chem. Phys. Lett.* **1978**, *54*, 373−377.

(24) Schoen, P. E.; Marrone, M. J.; Schnur, J. M.; Goldberg, L. S. Picosecond UV Photolysis and Laser-Induced Fluorescence Probing of Gas-Phase Nitromethane. *Chem. Phys. Lett.* **1982**, *90*, 272−276.

(25) Lee, C.; Yang, W.; Parr, R. G. Development of the Colle−Salvetti Correlation-Energy Formula into a Functional of the Electron Density. *Phys. Rev. B* **1988**, *37*, 8785−8789.

(26) Manaa, M. R.; Fried, L. E. Intersystem Crossings in Model Energetic Materials. *J. Phys. Chem. A* **1999**, *103*, 9349−9354.

(27) Kuklja, M. M.; Aduev, B. P.; Aluker, E. D.; Krasheninin, V. I.; Krechetov, A. G.; Mitrofanov, A. Y. Role of Electronic Excitations in Explosive Decomposition of Solids. *J. Appl. Phys.* **2001**, *89*, 4156−4166.

(28) Arenas, J. F.; Otero, J. C.; Peláez, D.; Soto, J. Photodissociation Mechanism of Nitramide: A CAS-SCF and MS-CASPT2 Study. *J. Phys. Chem. A* **2005**, *109*, 7172−7180.

(29) Borges, I., Jr. Excited Electronic and Ionized States of the Nitramide Molecule, H_2NNO_2, Studied by the Symmetry-Adapted-Cluster Configuration Interaction Method. *Theor. Chem. Acc.* **2008**, *121*, 239−246.

(30) Mialocq, J. C.; Stephenson, J. C. Picosecond Laser Study of the Collisionless Photodissociation of Dimethylnitramine at 266 nm. *Chem. Phys. Lett.* **1986**, *123*, 390−393.

(31) Tully, J. C. Molecular Dynamics with Electronic Transitions. *J. Chem. Phys.* **1990**, *93*, 1061−1071.

(32) Hammes-Schiffer, S.; Tully, J. C. Proton Transfer in Solution: Molecular Dynamics with Quantum Transitions. *J. Chem. Phys.* **1994**, *101*, 4657−4667.

(33) Fabiano, E.; Keal, T. W.; Thiel, W. Implementation of Surface Hopping Molecular Dynamics Using Semiempirical Methods. *Chem. Phys.* **2008**, *349*, 334−347.

(34) Weber, W. *Ein Neues Semiempirisches NDDO-Verfahren mit Orthogonalisierungskorrekturen: Entwicklung des Modells, Implementierung, Parametrisierung und Anwendungen*. Ph.D. Thesis, Universität Zürich, Zürich, Switzerland 1996.

(35) Weber, W.; Thiel, W. Orthogonalization Corrections for Semiempirical Methods. *Theor. Chem. Acc.* **2000**, *103*, 495−506.

(36) Otte, N.; Scholten, M.; Thiel, W. Looking at Self-Consistent-Charge Density Functional Tight Binding from a Semiempirical Perspective. *J. Phys. Chem. A* **2007**, *111*, 5751−5755.

(37) Barbatti, M.; Lan, Z.; Crespo-Otero, R.; Szymczak, J. J.; Lischka, H.; Thiel, W. Critical Appraisal of Excited State Nonadiabatic

Dynamics Simulations of 9H-Adenine. *J. Chem. Phys.* **2012**, *137*, 22A503.

(38) Lan, Z.; Fabiano, E.; Thiel, W. Photoinduced Nonadiabatic Dynamics of Pyrimidine Nucleobases: On-the-Fly Surface-Hopping Study with Semiempirical Methods. *J. Phys. Chem. B* **2009**, *113*, 3548−3555.

(39) Weingart, O.; Lan, Z.; Koslowski, A.; Thiel, W. Chiral Pathways and Periodic Decay in *cis*-Azobenzene Photodynamics. *J. Phys. Chem. Lett.* **2011**, *2*, 1506−1509.

(40) Zhang, W.; Lan, Z.; Sun, Z.; Gaffney, K. J. Resolving Photo-Induced Twisted Intramolecular Charge Transfer with Vibrational Anisotropy and TDDFT. *J. Phys. Chem. B* **2012**, *116*, 11527−11536.

(41) Lan, Z.; Lu, Y.; Weingart, O.; Thiel, W. Nonadiabatic Decay Dynamics of a Benzylidene Malononitrile. *J. Phys. Chem. A* **2012**, *116*, 1510−1518.

(42) Cui, G.; Thiel, W. Nonadiabatic Dynamics of a Truncated Indigo Model. *Phys. Chem. Chem. Phys.* **2012**, *14*, 12378−12384.

(43) Thiel, W. *MNDO Program*, version 6.1; Max-Planck-Institut für Kohlenforschung: Mülheim an der Ruhr, Germany, 2007.

(44) Ahlrichs, R.; Bär, M.; Häser, M.; Horn, H.; Kölmel, C. Electronic Structure Calculations on Workstation Computers: The Program System Turbomole. *Chem. Phys. Lett.* **1989**, *162*, 165−169.

(45) Koslowski, A.; Beck, M. E.; Thiel, W. Implementation of a General Multireference Configuration Interaction Procedure with Analytic Gradients in a Semiempirical Context Using the Graphical Unitary Group Approach. *J. Comput. Chem.* **2003**, *24*, 714−726.

(46) Glushkov, V. N. Partially Restricted Hartree-Fock Method for Singlet Excited States. *Opt. Spectrosc.* **2001**, *91*, 196−202.

(47) Bearpark, M. J.; Robb, M. A.; Bernhard Schlegel, H. A Direct Method for the Location of the Lowest Energy Point on a Potential Surface Crossing. *Chem. Phys. Lett.* **1994**, *223*, 269−274.

(48) Yarkony, D. R. Diabolical Conical Intersections. *Rev. Mod. Phys.* **1996**, *68*, 985−1013.

(49) Keal, T.; Koslowski, A.; Thiel, W. Comparison of Algorithms for Conical Intersection Optimisation Using Semiempirical Methods. *Theor. Chem. Acc.* **2007**, *118*, 837−844.

(50) Fabiano, E.; Thiel, W. Nonradiative Deexcitation Dynamics of 9H-Adenine: An OM2 Surface Hopping Study. *J. Phys. Chem. A* **2008**, *112*, 6859−6863.

(51) Becke, A. D. Density-Functional Thermochemistry. III. The Role of Exact Exchange. *J. Chem. Phys.* **1993**, *98*, 5648−5652.

(52) Stephens, P. J.; Devlin, F. J.; Chabalowski, C. F.; Frisch, M. J. Ab Initio Calculation of Vibrational Absorption and Circular Dichroism Spectra Using Density Functional Force Fields. *J. Phys. Chem.* **1994**, *98*, 11623−11627.

(53) Perdew, J. P.; Burke, K.; Ernzerhof, M. Generalized Gradient Approximation Made Simple. *Phys. Rev. Lett.* **1996**, *77*, 3865−3868.

(54) Perdew, J. P.; Ernzerhof, M.; Burke, K. Rationale for Mixing Exact Exchange with Density Functional Approximations. *J. Chem. Phys.* **1996**, *105*, 9982−9985.

(55) Ernzerhof, M.; Scuseria, G. E. Assessment of the Perdew−Burke−Ernzerhof Exchange-Correlation Functional. *J. Chem. Phys.* **1999**, *110*, 5029−5036.

(56) Adamo, C.; Barone, V. Toward Reliable Density Functional Methods without Adjustable Parameters: The PBE0 Model. *J. Chem. Phys.* **1999**, *110*, 6158−6170.

(57) Ernzerhof, M.; Perdew, J. P.; Burke, K. Coupling-Constant Dependence of Atomization Energies. *Int. J. Quantum Chem.* **1997**, *64*, 285−295.

(58) Weigend, F.; Ahlrichs, R. Balanced Basis Sets of Split Valence, Triple Zeta Valence and Quadruple Zeta Valence Quality for H to Rn: Design and Assessment of Accuracy. *Phys. Chem. Chem. Phys.* **2005**, *7*, 3297−3305.

(59) Weigend, F. Accurate Coulomb-Fitting Basis Sets for H to Rn. *Phys. Chem. Chem. Phys.* **2006**, *8*, 1057−1065.

(60) Pople, J. A.; Binkley, J. S.; Seeger, R. Theoretical Models Incorporating Electron Correlation. *Int. J. Quantum Chem.* **1976**, *10*, 1−19.

(61) Krishnan, R.; Pople, J. A. Approximate Fourth-Order Perturbation Theory of the Electron Correlation Energy. *Int. J. Quantum Chem.* **1978**, *14*, 91−100.

(62) Bartlett, R. J.; Purvis, G. D. Many-Body Perturbation Theory, Coupled-Pair Many-Electron Theory, and the Importance of Quadruple Excitations for the Correlation Problem. *Int. J. Quantum Chem.* **1978**, *14*, 561−581.

(63) Bartlett, R. J.; Silver, D. M. Many-Body Perturbation Theory Applied to Electron Pair Correlation Energies. I. Closed-Shell First-Row Diatomic Hydrides. *J. Chem. Phys.* **1975**, *62*, 3258−3268.

(64) Smith, B. J.; Radom, L. Calculation of Proton Affinities Using the G2(MP2,SVP) Procedure. *J. Phys. Chem.* **1995**, *99*, 6468−6471.

(65) Curtiss, L. A.; Redfern, P. C.; Smith, B. J.; Radom, L. Gaussian-2 (G2) Theory: Reduced Basis Set Requirements. *J. Chem. Phys.* **1996**, *104*, 5148−5152.

(66) Schirmer, J. Beyond the Random-Phase Approximation: A New Approximation Scheme for the Polarization Propagator. *Phys. Rev. A* **1982**, *26*, 2395−2416.

(67) Costain, W.; Cox, E. G. Structure of Dimethylnitramine. *Nature* **1947**, *160*, 826−827.

(68) Stolevik, R.; Rademach., P. Electron Diffraction of Structure of Dimethylnitramine $(CH_3)_2NNO_2$. *Acta Chem. Scand.* **1969**, *23*, 672−682.

(69) Domcke, W.; Yarkony, D. R.; Koeppel, H. *Conical Intersections: Electronic Structure, Dynamics and Spectroscopy*; World Scientific: Singapore, 2004.

(70) McQuaid, M. J.; Sausa, R. C. Absorption Cross Sections of Gaseous Dimethylnitramine at Selected Wavelengths between 185 and 325 nm. *Appl. Spectrosc.* **1991**, *45*, 916−917.

(71) Bhattacharya, A.; Guo, Y. Q.; Bernstein, E. R. Nonadiabatic Reaction of Energetic Molecules. *Acc. Chem. Res.* **2010**, *43*, 1476−1485.